PCCP

Ce K edge XAS of ceria-based redox materials under realistic conditions for the two-step solar thermochemical dissociation of water and/or CO2

Journal:	*Physical Chemistry Chemical Physics*
Manuscript ID:	CP-ART-06-2015-003179.R2
Article Type:	Paper
Date Submitted by the Author:	27-Aug-2015
Complete List of Authors:	Rothensteiner, Matthäus; Paul Scherrer Institute, ; ETH Zurich, Chemical and Bioengineerging Sala, Simone; Paul Scherrer Institute, Bonk, Alexander; EMPA, Laboratory for Hydrogen and Energy Vogt, Ulrich; Empa, Laboratory for Hydrogen and Energy Emerich, Hermann; Swiss Norwegian Beamlines (SNBL), van Bokhoven, Jeroen; Paul Scherrer Institute, ; ETH Zurich, Chemical and Bioengineerging

Ce K edge XAS of ceria-based redox materials under realistic conditions for the two-step solar thermochemical dissociation of water and/or CO_2

Matthäus Rothensteiner[*§] Simone Sala[*] Alexander Bonk[†]
Ulrich Vogt[†] Hermann Emerich[‡] Jeroen A. van Bokhoven[*§]

August 27, 2015

Abstract

X-ray absorption spectroscopy was used to characterise ceria-based materials under realistic conditions present in a reactor for solar thermochemical two-step water and carbon dioxide splitting. A setup suitable for *in situ* measurements in transmission mode at the cerium K edge from room temperature up to 1773 K is presented. Time-resolved X-ray absorption near-edge structure (XANES) data, collected for a 10 mol% hafnium-doped ceria sample ($Ce_{0.9}Hf_{0.1}O_{2-\delta}$) during reduction at 1773 K in a flow of inert gas and during re-oxidation by CO_2 at 1073 K, enables the quantitative determination of the non-stoichiometry δ of the fluorite-type structure. XANES analysis suggests the formation of the hexagonal Ce_2O_3 phase upon reduction in 2% hydrogen/helium at 1773 K. we discuss the experimental limitations and possibilities of high-temperature *in situ* XAS at edges of lower energy as well as the importance of the technique for understanding and improving the properties of ceria-based oxygen storage materials for thermochemical solar energy conversion.

[*]Paul Scherrer Institut 5232 Villigen PSI, Switzerland
[†]EMPA Überlandstrasse 129 CH-8600 Dübendorf, Switzerland
[‡]ESRF 6 rue Jules Horowitz BP 220 F-38043 Grenoble Cedex, France
[§]Institute for Chemical and Bioengineering ETH Zürich, Vladimir-Prelog-Weg 2, 8093 Zürich, Switzerland E-mail: jeroen.vanbokhoven@chem.ethz.ch

1 Introduction

At elevated temperatures and under reducing conditions, cerium dioxide reaches a high level of non-stoichiometry $CeO_{2-\delta}$ while maintaining its fluorite-type structure[1]. The formation of dioxygen (O_2 (g)), oxygen vacancies ($\ddot{V}_O$) and Ce^{3+} defects (Ce'_{Ce}) from Ce^{4+} cations (Ce_{Ce}) and O^{2-} anions (O_O) is described in equation 1 with Kröger-Vink notation. The high mobility of those vacancies and the capacity to reversibly bind and release oxygen with fast kinetics mean that ceria is of great importance for a large number of applications that require the activation, transport and storage of oxygen. In heterogeneous catalysis ceria-based oxides are applied as reducible supports for oxygen storage and activation, in three-way catalytic converters for the abatement of combustion engine exhaust gas, and in preferential oxidation (PROX) catalysts[2]. Electrochemical applications of ceria-based materials include its use as electrolytes in solid oxide fuel cells (SOFCs)[3]. The chemical (ambipolar) diffusion coefficient of oxygen in 15% samarium doped ceria falls in the range $1.7 \cdot 10^{-5}$ to $1.1 \cdot 10^{-4}$ $cm^2 s^{-1}$ at 1073 K and within $2.1 \cdot 10^{-4}$ to $3.6 \cdot 10^{-4}$ $cm^2 s^{-1}$ at 1773 K[4].

$$2Ce_{Ce} + O_O \longrightarrow 2Ce'_{Ce} + \ddot{V}_O + \frac{1}{2}O_2(g) \tag{1}$$

In the case of hydrogen production, a two-step redox cycle exploiting the oxygen storage capacity $\Delta\delta = \delta_{red} - \delta_{ox}$ of $CeO_{2-\delta}$ was first desribed by Otsuka et al.[5]. The Ce^{3+}/Ce^{4+} redox cycle can be driven by high-temperature heat from concentrated solar radiation and enables splitting of water into its elements (equation 2) and/or carbon dioxide into carbon monoxide and oxygen (equation 3), thereby converting and storing solar energy in chemical bonds in a manner first proposed and demonstrated experimentally by Abanades et al.[6,7]. The first partial reaction of the thermochemical looping process is the endothermal reduction of ceria (equation 4), usually performed at 1773 K. The second partial reaction – closing the redox cycle – is the exothermal oxidation of ceria (equations 5 and 6), which is performed at the same or at lower temperatures.

$$\Delta\delta H_2O \xrightarrow{CeO_{2-\delta}} \frac{\Delta\delta}{2}O_2 + \Delta\delta H_2 \tag{2}$$

$$\Delta\delta CO_2 \overset{CeO_{2-\delta}}{\longrightarrow} \frac{\Delta\delta}{2}O_2 + \Delta\delta CO \quad (3)$$

$$CeO_{2-\delta_{ox}} \overset{1773K}{\longrightarrow} CeO_{2-\delta_{red}} + \frac{\Delta\delta}{2}O_2 \quad (4)$$

$$CeO_{2-\delta_{red}} + \Delta\delta H_2O \longrightarrow CeO_{2-\delta_{ox}} + \Delta\delta H_2 \quad (5)$$

$$CeO_{2-\delta_{red}} + \Delta\delta CO_2 \longrightarrow CeO_{2-\delta_{ox}} + \Delta\delta CO \quad (6)$$

Sweep gas with a low oxygen content is used to charge and discharge the reactor containing the ceramic redox material. A solar cavity receiver reactor was used in the first demonstration on a technical scale by Chueh et al.[8].

The oxygen storage capacity $\Delta\delta$ of the redox material is pivotal for the overall efficiency of the process as well as the recovery of sensible heat, which also depends on the mode of operation: isothermal or with a temperature swing between reduction and re-oxidation. The energy conversion efficiency and the ideal design and mode of operation of high temperature solar thermochemical looping reactors are still under debate[9–13]. Thermodynamic analysis based on published data[14,15] indicates that advanced redox materials for this process must exhibit similar structural stability and kinetics but a higher $\Delta\delta$ at lower reduction temperatures and higher oxygen partial pressure than pure ceria to improve efficiency and economical viability[13,16].

Many attempts at optimization have been made to increase the solar-to-fuel energy conversion efficiency of the process: 1) to improve intrinsic properties of the material such as higher oxygen storage capacity $\Delta\delta$ and higher reaction rates by doping (e.g. Kaneko et al.[17]) and 2) improve properties of heat and mass transfer by using macroporous structures (e.g. Rudisill et al.[18]). Of fundamental importance in the quest for better materials is their stability upon exposure to a very large number of thermochemical redox cycles.

There is little experimental evidence on the nature of the electronic and geometric structure of ceria-based materials under the harsh conditions perpetuated by a solar thermochemical looping reactor. A large number of intermediary phases were found for ceria[15], but were not visible in XRD patterns collected by Abanades et al.[6]. The determination of element structure-property relationships in more complex ceria-based

mixed oxides is our motivation for building an *in situ* cell for X-ray absorption spectroscopy that can withstand the extreme conditions in a solar thermochemical reactor.

2 *In situ* XAS under relevant solar reactor conditions

X-ray absorption spectroscopy (XAS) is a powerful technique for determining the electronic and geometric structure of functional materials under relevant operating conditions [19,20]. The challenge faced in construction of a high temperature *in situ* cell capable of mimicking conditions in a solar thermochemical looping reactor, is to guarantee the access of photons of the required energies to a sample with an appropriate stable geometry in a well-known environment of uniform temperature and under a controlled gas flow. Equipment for *in situ* XAS up to 1273 K is readily available and cell designs for catalytic systems are helpfully reviewed by Bare and Ressler[21]. Guilera et al.[22] described cells for transmittance and fluorescence where reactive gases are employed, Huwe et al.[23] and An et al.[24] described cells for temperatures up to 1273 K. Above this temperature, however, *in situ* XAS data are hardly available because mechanically stable and inert materials that are permeable to X-rays are very limited. This is also the case for advanced techniques based on X-ray emission detection with more demanding X-ray optics, such as; high energy resolution fluorescence detection (HERFD)[25], high energy resolution off-resonant spectroscopy (HEROS)[26], or resonant inelastic X-ray scattering (RIXS)[27]. Approaches to performing spectroscopic measurements at significantly higher temperatures have been reported. A small sample may be placed on a resistive heating wire (e.g. Richet et al.[28], Neuville et al.[29]), which is limited by the melting point of the wire material. Another approach overcomes this limitation by heating an aerodynamically levitated sample with a laser (Landron et al.[30,31], Hennet et al.[32]).

The requirements of an *in situ* XAS flow cell with a controlled atmosphere (inert gas, water and/or CO_2) that may be used up to 1773 K, strongly restrict the choice of materials and geometry. Moreover, it is preferable to measure pure samples as preparation of pellets with diluent (for adjusting the absorption edge jump and transmission)

will probably result in contamination. Considering the low transmission of potential wall materials of such an *in situ* cell, (e.g. boron nitride, aluminium nitride and alumina) and the small unit edge step absorption length of ceria of $\approx 5\ \mu m$ at the cerium L_{III} edge (5.723 keV), it is more promising to perform *in situ* XAS measurements in transmission mode at the cerium K edge (40.443 eV) because there, the unit edge step absorption length of ceria is $\approx 80\ \mu m$. Uniform, self-supporting pellets of this thickness are fairly easy to prepare.

Paun and Safonova et al.[33] determined the concentration of Ce^{3+} in ceria nanoparticles with narrow size distributions by means of cerium K edge XANES. A shift in the edge position of a Ce^{3+} reference compound by -6.2 eV relative to a Ce^{4+} reference compound illustrates that K edge XAS is a sensitive tool for the determination of the electronic structure. HERFD-XAS at the cerium L_{III} edge revealed the dependence of spectral features on particle size. Kaneko et al.[34] reported cerium L_{III} edge XAS data of reduced and oxidised ceria mixed oxides before and after exposure to thermochemical cycling. Bessa et al.[35] determined the oxidation state of cerium in a catalyst for methane steam reforming from cerium L_{III} edge XANES spectra acquired *in situ* in fluorescence mode. They found a larger amount of Ce^{3+} due to the presence of Sm_2O_3 in a Rh/Sm_2O_3-ceria-alumina catalyst.

Yamamoto et al.[36] reported cerium L_{III} and zirconium K-edge time-resolved energy-dispersive *in situ* XAS of a ceria-zirconia supported Pt catalyst under reducing (hydrogen) and oxidising (oxygen) conditions up to 773 K. Rodriguez et al.[37] reported cerium L_{III} and Zr K edge XAS of this system. The tetragonal-to-cubic transition of ceria-zirconia solid solutions was investigated by EXAFS analysis up to 1073 K by Acuna et al.[38]. The distribution of oxygen vacancies doped ceria materials was investigated by XRD, K and L edge EXAFS by Deguchi et al.[39] and Nitani et al.[40]. Lee et al.[41] described typical margins of error for the first oxygen shell by fitting K edge EXAFS data, whereas Zhang et al.[42] compared results of XPS and L edge XAS to determine the Ce^{3+} concentration in ceria nanocrystals.

Cerium is coordinated eight-fold by oxygen atoms occupying the tetrahedral positions of the fluorite-type structure. The formation of an oxygen vacancy described in

Table 1: Expected changes in cerium K edge XAFS features related to non-stoichiometry in fluorite-type $CeO_{2-\delta}$.

Equation	value at 10^{-6} bar oxygen, 1773 K ($\delta = 0.1$)
$\Delta N^1_{Ce-O} = -4 \cdot \delta$	-0.4
$\Delta E = -6.2 \cdot 2\delta$ eV	-1.24 eV

equation 1 leads to an energy shift in the edge position and a reduction of the Ce-O co-ordination number. Table 1 summarizes the relationship between the non-stoichiometry δ and expected cerium K edge XAFS features. These data indicate that even at the highest non-stoichiometry relevant for a solar thermochemical looping process, the corresponding spectral changes are small in both the XANES and the EXAFS. It is thus very difficult to detect and quantify related structural changes, particularly under non-ambient conditions.

At high temperature substantial damping of the EXAFS signal significantly limits the access to structural information. In the case of a flat EXAFS region, however, the preferred strategy is to exploit spectral features in the XANES which are less affected by thermal damping. In contrast to the cerium L_{III} near edge region, which has more complex and oxidation-state-dependent spectral features, the shift in the edge position relates only to the oxidation state at the cerium K edge. Here, we describe *in situ* cerium K edge XAS under relevant solar reactor conditions for splitting of CO_2 up to 1773 K.

3 Experimental details

3.1 Preparation of material

$Ce_{0.9}Hf_{0.1}O_{2-\delta}$ was synthesized using ceria (Sigma Aldrich, 99.9%, $< 5\mu m$) and HfO_2 (Alfa Aesar, 99.95%). De-agglomeration and mixing were carried out by conventional ball milling on a roller mill (ZO, RM1) for 24 h in polypropylene bottles using YSZ balls 5 mm in diameter (Tosoh). After 24 h the slurry was separated from the YSZ balls and dried at 358 K for 12 h. Samples of 15 mg were pressed uni-axially at 5 kN in a 6 mm pressing tool. The pellets were fired in a furnace (Carbolite HTF 17/10) at 1873 K

for 5 h in air on a ceria powder to avoid contamination.

3.2 *In situ* XAS experiments

In situ XAS experiments were carried out at beam line BM01B of the Swiss-Norwegian Beamlines (SNBL) at the European Synchrotron Radiation Facility (ESRF) in Grenoble, France. BM01B at SNBL is a multi-technique beam line for combined in situ X-ray diffraction, X-ray absorption and Raman scattering experiments[43]. An unusually small gap between the first and the second monochromator crystal enables measurements from the Ti K to the Au K edges in one single Bragg rotation using a Si (111) crystal. The divergence of the beam is approximately twice as large as the Darwin width. Taking into account both the intrinsic contribution of the Si-111 monochromator crystal and the divergence[44], the energy resolution ΔE of the instrument at 40 keV is better or equal to 6.0 eV. The incident and transmitted intensities were monitored with ionization chambers filled with 1 bar krypton/argon (20/80%) and 1.2 bar krypton that were before and after the *in situ* cell, respectively. A pellet of ceria in cellulose was placed between the second and third ionization chamber as a reference. The storage ring (6 GeV) was operated in 16 bunch filling mode at 90 mA intensity and 10 h life-time. Measurements were carried out in transmission mode at the cerium K edge (40.433 keV) with a step width of 1 eV and 100 ms step time. The monochromator was detuned to suppress higher-order harmonics. Spectra of the XANES region (40.2 to 41 keV) with a step width of 1 eV were recorded with a time resolution of 0.676 min^{-1}. Spectra of the EXAFS region (40.2 to 42 keV) were recorded at room temperature with a step width of 1 eV.

A 10 mg pellet (diameter 5 mm) was introduced into the cell. Samples were exposed to reducing conditions (1 atm argon or 2% H_2 in helium) and oxidising conditions (1 atm CO_2) at a gas flow rate of 100 mL min^{-1}. The rate of heating was 50 $K{\cdot}min^{-1}$, cooling to 1073 K - 100 $K{\cdot}min^{-1}$; cooling from 1073 K to room temperature was achieved by switching off the furnace. Gases used were; Ar (BIP, Air Products, O_2 < 10 ppb water < 20 ppb CO + CO_2 < 100 ppb THC (as CH_4) < 100 ppb N_2 < 1 ppm), CO_2 4.5, 2% H_2 5.0 in He 5.0 (Messer France SAS).

3.3 Data processing

Normalisation by a standard procedure and further data treatment were performed using Matlab code. The energy shift in the edge position ΔE was extracted by spline interpolation of golay-filtered normalised spectra at an absorption value of 0.746 corresponding to the edge position of the first spectrum. Geometrically, this corresponds to the intersection of the rising absorption curves with a line parallel to the energy axis. The non-stoichiometry δ was calculated by assuming a linear relationship between ΔE and the Ce^{3+} concentration, and hafnium consistently present as Hf^{4+}. The noise level in the reference spectra did not allow for the correction of possible energy drifts by alignment of reference spectra.

3.4 High-temperature *in situ* XAS cell

Figure 1 shows a schematic representation of our setup for XAS measurements in transmission mode, including the high-temperature XAS cell and a photograph of an alumina sample holder. The main components are two mass flow controllers (Bronkhorst) for dosing reducing and oxidizing gases, a 4-way valve (Vici) that enables a rapid switch from reducing to oxidizing atmospheres and vice versa, the tubular *in situ* cell, which is heated with an infrared furnace (Ulvak VHT E44), and a mass spectrometer (MS, Pfeiffer Ominstar GSD 320) for on-line analysis of the composition of the product gas.

The *in situ* cell consists of an alumina tube (99.7 Alsint, Haldenwanger Ceramics, 9.5 mm x 12.7 mm x 400 mm). The ends of the tube are connected to steel adapters for 12 mm swagelok tubes. The inlet and the outlet were manufactured by modifying 12 mm swagelok linear connectors. In the cell, the temperature in the hot zone (100 mm) was measured at the position of the sample with an S-type (Pt/Rh) thermocouple covered by an alumina sheath. The conditions that can be reached in the cell are given in Table 2. Samples are introduced on an alumina sample holder consisting of two cylindrical parts. The inner diameter (3.5 mm) of the sample holder determines the maximum cross section of the X-ray beam on the sample. The X-ray beam is parallel

Table 2: Characteristics of the setup for *in situ* XAS under realistic two-step solar thermochemical water- and CO_2-splitting conditions.

Parameter	value
Temperature range	room temperature to at least 1773 K
Inner diameter (cell)	9.5 mm
Volume	35 mL
Cross sectional diameter of beam on sample	$<$ 3.4 mm

to the axis of the *in situ* cell and passes through removable 1 mm thick PTFE windows at the inlet and outlet. The cell withstands isothermal CO_2 and water splitting conditions as well as reducing atmospheres (5% hydrogen/helium) and allows fast cycling between reducing and oxidizing conditions at high rates of heating and cooling and temperatures from room temperature up to at least 1773 K. Heating and cooling rates of several hundred K·min^{-1} can be reached due to the power of the IR furnace and the small thermal mass of the cell. Rates of heating and cooling are primarily limited by resistance to thermal shock. The total inner volume of the cell is 35 mL. Given the small amount of sample of typically 10 to 15 mg, the rather large dead volume represents a drawback, but can be compensated for using high gas flows. The *in situ* cell is placed between the first (I_0) and second (I_{T1}) ionization chambers. A reference material exposed to ambient conditions and located between the second and third ionization chamber is measured simultaneously. The same cell is used for material testing in the home laboratory.

4 Results and Discussion

Figure 2(a) illustrates normalised cerium K edge spectra of $Ce_{0.9}Hf_{0.1}O_{2-\delta}$ at 298, 1073 and 1773 K at three different levels of non-stoichiometry δ. Spectra were recorded during two-step CO_2-splitting with a temperature swing between 1773 and 1073 K, under isothermal conditions for CO_2 splitting at 1773 K and after reduction with hydrogen at 1773 K. After reduction a shift in the edge position to lower photon energy was found at all temperatures, indicating the accessibility of structural information related to the near edge region of the spectra up to 1773 K. As indicated by the data in Table 1, the

expected edge shift is small after reduction in a flow of argon and larger after reduction in hydrogen.

The valence of cerium and the corresponding non-stoichiometry δ can be determined from the relative energy shift in the edge position, which is an accurate measure of oxidation state under ambient conditions[33]. A simple but effective method to capture these energy shifts is to measure the energy of the spectra at constant normalised absorption. In normalised spectra, damping leads to an apparent shift in the edge position to lower energies. Despite temperature differences of 1575 K, the accuracy of the edge position is remarkably good without any correction for temperature. Below is a discussion of the effect of temperature on the shift in the edge position.

The amplitude of the extended X-ray absorption fine structure is strongly affected by damping because of thermal and structural disorder. As the temperature increases, the useful range for EXAFS analysis becomes smaller, as the energy range in which oscillations are distinguishable from noise moves close to the absorption edge. While oscillatory features are still visible at 1073 K, the post edge region contains only very weak oscillations at 1773 K. Furthermore, anharmonic oscillations hinder a detailed EXAFS analysis[45,46]. Therefore, we did not attempt to fit EXAFS at high temperature.

After reduction in hydrogen, both the shift in the edge position and the spectral features suggest the formation of the hexagonal Ce_2O_3 phase. In this crystal structure, cerium is surrounded by seven oxygen atoms. The relationship between non-stoichiometry and coordination number given in Table 1 is valid only for the cubic, fluorite-type phase of ceria.

Figure 3 displays the results of the completed experiment. It gives the temperature in the reactor, the gas atmosphere, and the mass spectrometer signals for oxygen (m/z = 32) and water (m/z = 18) which form under reducing conditions in a flow of argon and 2% hydrogen/helium, respectively. Furthermore, Figure 3 shows the non-stoichiometry δ in $Ce_{0.9}Hf_{0.1}O_{2-\delta}$ and the corresponding energy of the edge shift obtained at constant normalised absorption. In addition, a contour plot of normalised difference spectra highlights minute spectral changes. A spectrum recorded at 1073 K after thermal reduction in a flow of argon at 1773 K was subtracted to obtain these difference spectra.

In the first part of the experiment, two redox cycles with a temperature swing were performed, consisting of a reduction step at 1773 K in a flow of argon followed by an oxidation step at 1073 K in a flow of CO_2. The MS signal shows that in the first cycle, while heating from room temperature, oxygen release starts at about 1323 K and peaks when the temperature reaches 1773 K. After cooling to 1073 K and re-oxidation in a flow of CO_2 at 1073 K, the same amount of oxygen is released from the material in the second cycle, indicated by an oxygen MS signal peak area ratio of 1.00, which suggests complete re-oxidation. The onset of the second oxygen peak occurs at the same temperature as in the first cycle but has a different peak shape, indicating that oxygen release is slower. The maximum oxygen concentration in the flush gas is lower and the peak broader. After the second re-oxidation at 1073 K, isothermal redox cycles were performed by heating up in CO_2 and switching between argon and CO_2 at 1773 K. When the temperature reached 1773 K, the oxygen signal presented as a small peak. After switching from CO_2 to argon the oxygen release from the sample was revealed by comparison with the MS signal obtained when the same switch was performed at 1073 K. The sample was then cooled to 298 K and another redox cycle with a temperature swing carried out. During heating 12% of the oxygen released in the first cycle was detected, confirming that this fraction of Ce^{3+} is oxidised to Ce^{4+} by residual oxygen.

In the second part of the experiment, the sample was reduced by heating from 1073 to 1773 K in a flow of 2% hydrogen in He. After cooling to 298 K, the temperature was increased to 1073 K in CO_2 followed by reduction at 1773 K in a flow of 2% hydrogen in helium and oxidation at 1073 K in CO_2. The MS signal for water clearly indicates that reduction of the sample begins to take place at 1073 K. A similar amount of water forms in the second reduction treatment with hydrogen. Heating from room temperature to 1073 K in CO_2 leads to re-oxidation, as proved by the formation of a CO peak at 28 m/z (not shown).

It is evident that the non-stoichiometry δ determined from XAS spectra is in good agreement with the MS signals reported above. The precision and noise of δ obtained from XAS can be estimated from the first six spectra of the pristine sample taken in a flow of argon at 298 K and the average of which is $6.886 \cdot 10^{-4}$ and a standard

deviation of $8.6 \cdot 10^{-3}$. The maximum value of δ in $Ce_{0.9}Hf_{0.1}O_{2-\delta}$ is 0.45 based on the assumption that hafnium is always present as Hf^{4+}.

The non-stoichiometry δ reaches a maximum value of 0.10 in the first reduction step. In the second reduction step, a slightly higher value (about 0.11) is reached. Prior to release of oxygen, as indicated by MS, δ rises to an apparent value of about 0.015, a behaviour that we ascribe to the effects of temperature. However, based on the non-stoichiometry after the second reduction step and the oxygen peak area ratio of 1.00 0.35 is assumed for this apparent δ. Results for δ of the second re-oxidation step are very similar and in line with the MS signals. Re-oxidation at 1073 K leads to a decrease in δ by 0.065 in the first and 0.08 in the second cycle. During cooling from 1773 K to 1073 K δ does not change significantly in the first two redox cycles. Upon switching to CO_2 at 1073 K the temporal evolution of the non-stoichiometry during re-oxidation is visible.

The general trends of the non-stoichiometry agree with the experimental conditions while heating to 1773 K in CO_2 and switching under isothermal conditions at 1773 K. However, lower values for δ are found in argon despite a similar amount of oxygen, shorter reduction times and probably higher CO_2 levels. The switch from argon to CO_2 at 1773 K leads to a decrease in δ by about 0.043 and increases by about the same value in the subsequent reduction step. Decreasing the temperature of the reduced sample in argon from 1773 K to 1073 K leads to 0.008 decrease in δ and a further decrease by 0.06 to 0.066 as the temperature reaches 298 K. These edge shifts are not caused by temperature changes and play only a small role. Subsequent heating leads to oxygen release, starting at about 1623 K, and is accompanied by a 0.035 increase in δ. This increase in δ was twice as high as expected based on oxygen peak area ratios and corresponding values for δ obtained earlier in the experiment and coinciding with a change in beam intensity due to refilling of the storage ring. During the last cooling step in argon to 1073 K δ further increases and eventually plateaus at 0.14. This value drops by 0.1 during re-oxidation in CO_2 at 1073 K.

Reduction in hydrogen leads to a clear increase in δ under isothermal conditions at 1073 K and after heating to 1773 K, reaching a maximum value of 0.44. The theoretical

maximum of δ is 0.45. Cooling from 1773 K to room temperature under reducing conditions lead to a decrease in δ from 0.44 to 0.40, as a result of temperature. This observation suggests that the extraction of the non-stoichiometry from XAS spectra recorded in the same gas environment at two temperatures separated by 1475 K, leads to an error of less than 10% without correcting for temperature effects. Re-oxidation is fast when heating from room temperature in CO_2, starting at approximately 873 K, and it is approximately 75% complete when the temperature in the reactor reaches 1073 K. The second reduction step in hydrogen is similar to the first. Upon re-oxidation after switching to CO_2 at 1073 K the change from a hexagonal to a cubic structure is very fast. However, re-oxidation is probably not completed when the heating of the furnace is stopped. At the end of the experiment, and under oxidizing conditions at room temperature, δ reaches an average value of 0.018. Apart from temperature effects and incomplete re-oxidation, this derivation might be explained by significant structural changes, such as the segregation of a hafnium-rich phase upon complete reduction in hydrogen. Absorption spectra before and after normalization are provided in the supporting information. Most important, changes in the total absorption and variations in the edge jump occur upon switching from argon to CO_2 and 2% hydrogen/helium. In the contour plot of difference spectra in Figure 3 it is possible to distinguish minima and maxima, indicating the reduced and oxidised state of ceria as well as the temperature in the reactor.

From 298 to 1773 K, temperature effects are also evident in the XANES region, which complicates the determination of non-stoichiometry. Interpolation at constant absorption is less affected by these influences than using the position of the maximum of the first derivative, but depends on the pre-and post-edge region for subtracting the background. The noise level related to the non-stoichiometry indicates that the experiment is highly dependent on the stability of the incoming X-ray beam and the mechanical movement of the monochromator crystals. The rocking curve is extremely narrow and the stability and reproducibility of the beam after detuning is limiting at a photon energy of 40 keV. An energy scan from 40 to 41 keV requires a mere 0.07 $^\circ$ change in the Si (111) Bragg angle. On the other hand, the energy of the beam can

be changed quickly, leading to better time resolution. XAS data measured at the $L_{II,III}$ edges, show more complex features related to the electronic structure of cerium. These features might be advantageous at high temperature, at which relevant features are observable only in the XANES region, but do require the use of a diluent such as boron nitride. Preliminary experiments (see supporting information) showed the possibility of measuring the cerium L_{III} edge in transmission mode, but chemical stability was not achieved at high temperatures. Measurements in transmission mode restrict XAS at the absorption edges of dopant elements due to their low concentrations (typically < 20 mol%) and the high absorption cross section of cerium.

The ceria-hafnia system has been considerably less explored than the ceria-zirconia system. High-temperature structural or thermodynamic data are available[47], however little work on non-stoichiometric compounds has been done. Zhou and Gorte et al.[48,49] reported on ceria-hafnia and found the separation of $Ce_{0.8}Hf_{0.2}O_2$ into $Ce_{0.81}Hf_{0.19}O_2$ and $Ce_{0.85}Hf_{0.15}O_2$ when calcined in air at 1323 K.

In a study on doped ceria compounds for thermochemical cycling[50], it was found that hafnium increases the non-stoichiometry less than zirconium. This is in line with work by Baidya et al.[51] who found that in equimolar composition ceria-hafnia is less reducible than ceria-zirconia. The catalytic properties of ceria-hafnia materials were investigated by Reddy et al.[52] who found higher catalytic activity in soot oxidation compared to ceria-zirconia materials.

The possibility to measure XAS at high photon energies such as the Hf K edge (65.351 keV) could provide complementary structural information. Combined with *in situ* XRD, our approach can contribute to a better understanding of ceria-based systems under extreme conditions.

Unlike well-established laboratory methods to determine the amounts of reduction and oxidation products, XAS provides element-specific electronic and geometric structural information and gives greater insight into redox chemistry. Several effects must be considered when working at high temperature. Radiative heat transfer predominates and thus the absorbance of the sample plays a crucial role. Dark samples such as praseodymium-doped ceria might reach a higher temperature than bright samples such

as pure ceria. The damping of the EXAFS signal, however, might offer the possibility of measuring the temperature of the sample. Our ultimate goal is to characterize materials for the thermochemical dissociation of water and CO_2. To achieve this it is necessary to determine the structural features that govern the formation, distribution, and reactivity of oxygen vacancies and, using this knowledge we hope to design materials with superior properties for the exchange and storage of oxygen. The cell described enables exposure of materials to relevant solar thermal conditions - in particular achieving desired temperature regimes for EXAFS measurements in their reduced state. A superior redox material must be able to store large amounts of oxygen by reacting with water or CO_2 with fast kinetics, high thermal stability and cyclability. An element-specific *in situ* method such as X-ray spectroscopy is necessary to determine structural changes during the production of solar fuels.

5 Conclusions

A cell was constructed for *in situ* X-ray absorption spectroscopy in transmission mode able to withstand the harsh conditions required for the thermochemical dissociation of water and/or CO_2 using non-stoichiometric ceria-based redox materials. Overall, ceria-based redox materials can be characterized *in situ* under relevant conditions using cerium K-edge X-ray absorption spectroscopy in transmission mode. Using diluted samples, the absorption L_{III} edge of cerium can be accessed. The high penetration depth of X-rays at the cerium K edge facilitates a simple and robust cell design that can be operated under these harsh conditions. In the temperature range relevant to thermochemical looping the determination of structural properties is, to a large extent, limited to spectral features in the XANES region of the spectrum. The shift in the cerium K edge position enables accurate determination of the non-stoichiometry. By means of our cell it is possible to determine the element-specific structural changes that occur during synthesis of solar fuel. This development will enrich current efforts to elucidate optimal element combinations in solar-fuel redox materials.

6 Acknowledgements

The authors thank Urs Hartfelder, Dr. Kim Meyer, Flavien Morel, René Kopelent and Fangjian Lin for assistance during beam times. Financial support by the Swiss Competence Center Energy & Mobility (CCEM) is gratefully acknowledged.

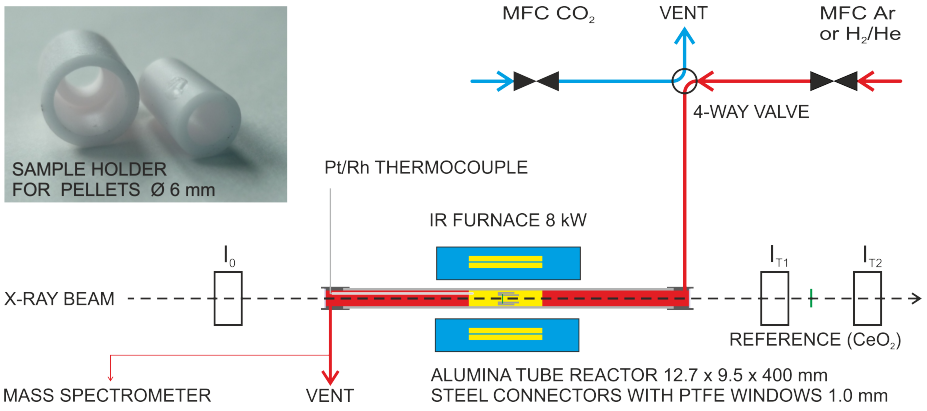

Figure 1: Setup for *in situ* XAS under realistic two-step solar thermochemical CO_2-splitting conditions. Top left: photograph of an alumina sample holder.

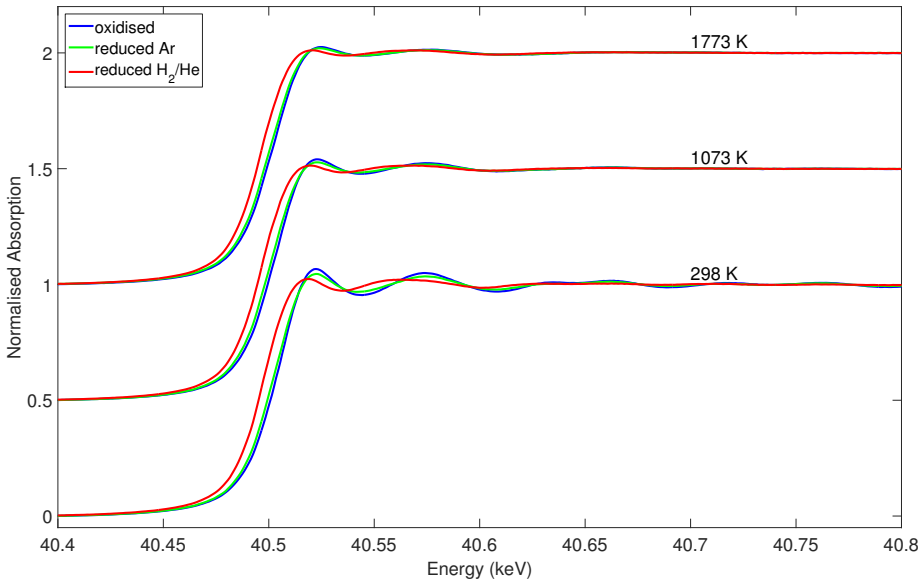

(a)

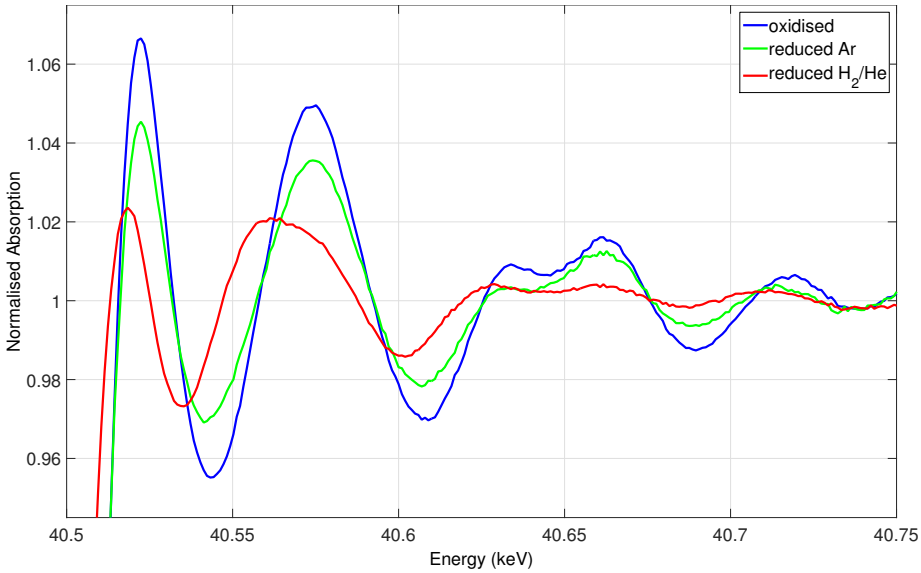

(b)

Figure 2: a) Normalised cerium K edge spectra of $Ce_{0.9}Hf_{0.1}O_{2-\delta}$, recorded at 298, 1073, and 1773 K. 'Oxidised' (298 K) is the spectrum of the as-prepared pellet after introduction into the XAS cell. 'Oxidised' (1073) and 'oxidised' (1773) were recorded after oxidation in 1 atm CO_2. 'Reduced Ar' denotes spectra recorded after reducing the sample in a flow of argon at 1773 K and 'reduced H_2/He' spectra recorded after reducing the sample in a flow of 2% hydrogen/helium at 1773 K. b) Close-up of spectra recorded at 298 K. 'Oxidised' denotes the spectrum of the as-prepared pellet after introduction into the XAS cell. 'Reduced Ar' denotes spectra recorded after reducing the sample in a flow of argon at 1773 K and 'reduced H_2' spectra recorded after reduction in a flow of 2% hydrogen/helium at 1773 K.

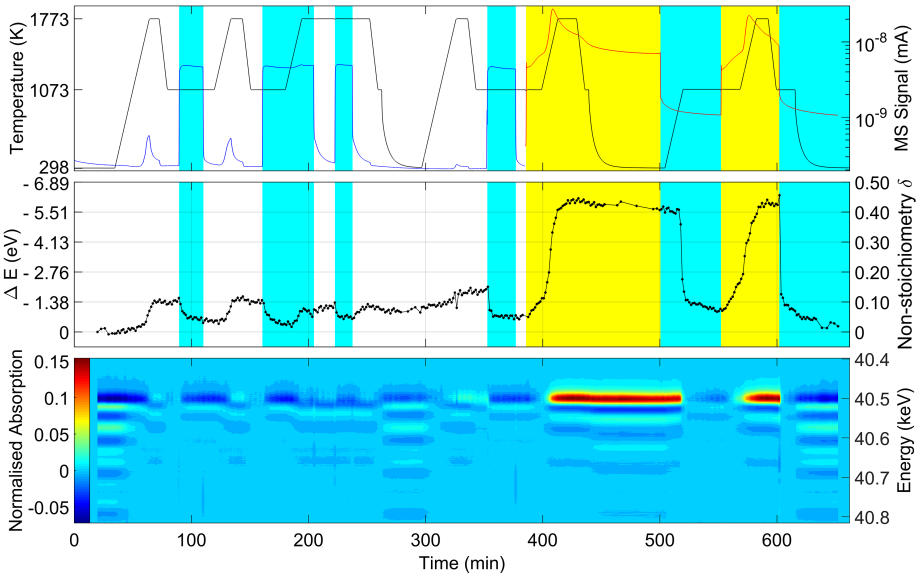

Figure 3: Top: Experimental conditions: furnace profile, gas atmosphere (white = argon, blue = CO_2, yellow = 2 % hydrogen/helium), MS signals for oxygen (blue) and water (red). Middle: Non-stoichiometry δ and corresponding shift of the edge energy, determined by interpolation at the absorption value corresponding to the edge position of the first spectrum Bottom: Contour plot of normalised difference spectra obtained by subtraction of a spectrum recorded at 1073 K after the first reduction by flushing the reactor with argon at 1773 K. See Figure 2 for selected XAS spectra.

References

[1] M. Mogensen, N. M. Sammes and G. A. Tompsett, *Solid State Ionics*, 2000, **129**, 63–94.

[2] A. Trovarelli, *Catal. Rev.*, 1996, **38**, 439–520.

[3] N. Q. Minh, *J. Am. Ceram. Soc.*, 1993, **76**, 563–588.

[4] W. C. Chueh and S. M. Haile, *Philos. Trans. A. Math. Phys. Eng. Sci.*, 2010, **368**, 3269–94.

[5] K. Otsuka, M. Hatano and A. Morikawa, *J. Catal.*, 1983, **79**, 493–496.

[6] S. Abanades and G. Flamant, *Sol. Energy*, 2006, **80**, 1611–1623.

[7] S. Abanades, P. Charvin, G. Flamant and P. Neveu, *Energy*, 2006, **31**, 2805–2822.

[8] W. C. Chueh, C. Falter, M. Abbott, D. Scipio, P. Furler, S. M. Haile and A. Steinfeld, *Science*, 2010, **330**, 1797–801.

[9] T. Rager, *Chem. Commun.*, 2012, **48**, 10520–10522.

[10] M. Roeb and C. Sattler, *Science*, 2013, **341**, 470–1.

[11] C. L. Muhich, B. W. Evanko, K. C. Weston, P. Lichty, X. Liang, J. Martinek, C. B. Musgrave and A. W. Weimer, *Science*, 2013, **341**, 540–2.

[12] Y. Hao, C.-K. Yang and S. M. Haile, *Phys. Chem. Chem. Phys.*, 2013, **15**, 17084–92.

[13] I. Ermanoski, J. E. Miller and M. D. Allendorf, *Phys. Chem. Chem. Phys.*, 2014, **16**, 8418–27.

[14] R. Panlener, R. Blumenthal and J. Garnier, *J. Phys. Chem. Solids*, 1975, **36**, 1213–1222.

[15] M. Zinkevich, D. Djurovic and F. Aldinger, *Solid State Ionics*, 2006, **177**, 989–1001.

[16] J. E. Miller, A. H. McDaniel and M. D. Allendorf, *Adv. Energy Mater.*, 2014, **4**, 1300469–1300469.

[17] H. Kaneko, T. Miura, H. Ishihara, S. Taku, T. Yokoyama, H. Nakajima and Y. Tamaura, *Energy*, 2007, **32**, 656–663.

[18] S. G. Rudisill, L. J. Venstrom, N. D. Petkovich, T. Quan, N. Hein, D. B. Boman, J. H. Davidson and A. Stein, *J. Phys. Chem. C*, 2013, **117**, 1692–1700.

[19] S. Bordiga, E. Groppo, G. Agostini, J. A. van Bokhoven and C. Lamberti, *Chem. Rev.*, 2013, **113**, 1736–850.

[20] C. Garino, E. Borfecchia, R. Gobetto, J. A. van Bokhoven and C. Lamberti, *Coord. Chem. Rev.*, 2014, **277-278**, 130–186.

[21] S. R. Bare and T. Ressler, *Chapter 6 - Characterization of Catalysts in Reactive Atmospheres by X-ray Absorption Spectroscopy*, Elsevier Inc., 1st edn, 2009, vol. 52, pp. 339–465.

[22] G. Guilera, B. Gorges, S. Pascarelli, H. Vitoux, M. A. Newton, C. Prestipino, Y. Nagai and N. Hara, *J. Synchrotron Radiat.*, 2009, **16**, 628–34.

[23] H. Huwe and M. Fröba, *J. Synchrotron Radiat.*, 2004, **11**, 363–5.

[24] P. An, C. Hong, J. Zhang, W. Xu and T. Hu, *J. Synchrotron Radiat.*, 2014, **21**, 165–9.

[25] J. Singh, E. M. C. Alayon, M. Tromp, O. V. Safonova, P. Glatzel, M. Nachtegaal, R. Frahm and J. A. van Bokhoven, *Angew. Chem. Int. Ed. Engl.*, 2008, **47**, 9260–4.

[26] J. Szlachetko, C. J. Milne, J. Hoszowska, J.-C. Dousse, W. BÅĆachucki, J. Sà, Y. Kayser, M. Messerschmidt, R. Abela, S. Boutet, C. David, G. Williams, M. Pajek, B. D. Patterson, G. Smolentsev, J. A. van Bokhoven and M. Nachtegaal, *Struct. Dyn.*, 2014, **1**, 021101.

[27] J. Szlachetko, J. Sá, O. Safonova, G. Smolentsev, M. Szlachetko, J. A. van Bokhoven and M. Nachtegaal, *J. Electron Spectros. Relat. Phenomena*, 2013, **188**, 161–165.

[28] P. Richet, P. Gillet, A. Pierre, M. A. Bouhifd, I. Daniel and G. Fiquet, *J. Appl. Phys.*, 1993, **74**, 5451.

[29] D. Neuville, L. Cormier, D. de Ligny, J. Roux, a M. Flank and P. Lagarde, *Am. Mineral.*, 2008, **93**, 228–234.

[30] C. Landron, X. Launay, J. Rifflet, P. Echegut, Y. Auger, D. Ruffier, J. Coutures, M. Lemonier, M. Gailhanou, M. Bessiere, D. Bazin and H. Dexpert, *Nucl. Instruments Methods Phys. Res. Sect. B Beam Interact. with Mater. Atoms*, 1997, **124**, 627–632.

[31] C. Landron, L. Hennet, J.-P. Coutures, T. Jenkins, C. AleÌĄtru, N. Greaves, A. Soper and G. Derbyshire, *Rev. Sci. Instrum.*, 2000, **71**, 1745.

[32] L. Hennet, V. Cristiglio, J. Kozaily, I. Pozdnyakova, H. E. Fischer, A. Bytchkov, J. W. E. Drewitt, M. Leydier, D. Thiaudière, S. Gruner, S. Brassamin, D. Zanghi, G. J. Cuello, M. Koza, S. Magazù, G. N. Greaves and D. L. Price, *Eur. Phys. J. Spec. Top.*, 2011, **196**, 151–165.

[33] C. Paun, O. V. Safonova, J. Szlachetko, P. M. Abdala, M. Nachtegaal, J. Sa, E. Kleymenov, A. Cervellino, F. Krumeich and J. A. van Bokhoven, *J. Phys. Chem. C*, 2012, **116**, 7312–7317.

[34] H. Kaneko and Y. Tamaura, *J. Phys. Chem. Solids*, 2009, **70**, 1008–1014.

[35] R. B. Duarte, O. V. Safonova, F. Krumeich, M. Makosch and J. A. van Bokhoven, *ACS Catal.*, 2013, **3**, 1956–1964.

[36] T. Yamamoto, A. Suzuki, Y. Nagai, T. Tanabe, F. Dong, Y. Inada, M. Nomura, M. Tada and Y. Iwasawa, *Angew. Chem. Int. Ed. Engl.*, 2007, **46**, 9253–6.

[37] J. A. Rodriguez, J. C. Hanson, J.-y. Kim, G. Liu, A. Iglesias-Juez and M. Fernández-García, *J. Phys. Chem. B*, 2003, **107**, 3535–3543.

[38] L. Acuna, D. Lamas, R. Fuentes, I. Fabregas, N. Walsoe de Reca, R. Prado, M. Fantini and A. Craievich, *LNLS 2007 Act. Rep.*, 2007, 1–2.

[39] H. Deguchi, H. Yoshida, T. Inagaki and M. Horiuchi, *Solid State Ionics*, 2005, **176**, 1817–1825.

[40] H. Nitani, T. Nakagawa, M. Yamanouchi, T. Osuki, M. Yuya and T. a. Yamamoto, *Mater. Lett.*, 2004, **58**, 2076–2081.

[41] J. Lee, M. Tang, W. Shih and R. Liu, *Mater. Res. Bull.*, 2002, **37**, 555–562.

[42] F. Zhang, P. Wang, J. Koberstein, S. Khalid and S.-W. Chan, *Surf. Sci.*, 2004, **563**, 74–82.

[43] W. van Beek, O. V. Safonova, G. Wiker and H. Emerich, *Phase Transitions*, 2011, **84**, 726–732.

[44] M. Sanchez del Rio and O. Mathon, *Adv. Comput. methods x-ray neutron Opt.*, 2004, **5536**, 157–164.

[45] A. Filipponi, *J. Phys. Condens. Matter*, 2001, **13**, R23–R60.

[46] E. Bus, J. T. Miller, a. J. Kropf, R. Prins and J. A. van Bokhoven, *Phys. Chem. Chem. Phys.*, 2006, **8**, 3248–58.

[47] H. Fujimori, M. Yashima, S. Sasaki, M. Kakihana, T. Mori, M. Tanaka and M. Yoshimura, *Phys. Rev. B*, 2001, **64**, 1–5.

[48] G. Zhou, P. R. Shah, T. Montini, P. Fornasiero and R. J. Gorte, *Surf. Sci.*, 2007, **601**, 2512–2519.

[49] G. Zhou and R. J. Gorte, *J. Phys. Chem. B*, 2008, **112**, 9869–9875.

[50] J. R. Scheffe, R. Jacot, G. R. Patzke and A. Steinfeld, *J. Phys. Chem. C*, 2013, **117**, 24104–24114.

[51] T. Baidya, M. S. Hegde and J. Gopalakrishnan, 2007, **2**, 5149–5154.

[52] B. M. Reddy, G. K. Reddy, L. H. Reddy and I. Ganesh, *Open Phys. Chem. J.*, 2009, **3**, 24–29.